J Mater Sci: Mater Electron (2022) 33:12371–12383

Investigation of structural and optical properties of lithium lead bismuth silicate glasses

Sumit Chauhan[1], Rajni Bala[1,*], Saroj Rani[2], and Sanjay Gaur[3]

[1] Department of Physics, Maharshi Dayanand University, Rohtak, Haryana 124001, India
[2] Government P. G. College, Panchkula, Haryana 134109, India
[3] Department of Physics, GDC Memorial College, Bahal, Bhiwani, Haryana 127028, India

Received: 11 January 2022
Accepted: 2 April 2022
Published online: 24 April 2022

ABSTRACT

Heavy metal-based oxide glasses with composition $30Li_2O{\cdot}20PbO{\cdot}xBi_2O_3{\cdot}(50-x)SiO_2$ (where, x = 0 to 50 mol%) were prepared by standard melt-quench procedure at temperature 1150 °C for 30 min. The amorphous nature of the prepared samples was confirmed by the low-intensity broad hump in XRD analysis. Fourier transform infrared spectroscopy predicts the role of Bi_2O_3 as network former as well as modifier due to the existence of BiO_3 and BiO_6 structural units. The Archimedes principle was used to compute the density of samples, which was found to increase with the bismuth concentration. The optical properties of synthesized samples were measured using UV–VIS–NIR spectroscopy. With increasing bismuth content, optical parameters such as cut-off wavelength, theoretical optical basicity, oxide ion polarizability, and molar refractivity increase, whereas the optical energy bandgap decreases. The large values of refractive index and smaller metallization criterion for all the samples (ranges from 0.310 to 0.395) suggest that studied glasses can be explored for non-linear optical applications.

1 Introduction

Numerous studies on heavy metal-based oxide glasses containing PbO, Bi_2O_3, and other heavy metals have revealed substantial non-resonant optical infrared transmission up to about 7 μm [1–3]. Glass materials have various advantages like as effortlessly molded in multiple shapes, smoothly constructed and manufactured, transparent, to be thermally stable and chemically robust, and cover vast compositional range [4–6], as compared to other materials. Due to its higher absorption of dopants in an amorphous state, glassy materials provide new opportunities for the fabrication of compact, high-power devices [7]. Silicates are generally considered to be necessary glassy host materials for a variety of opto-dielectric applications. SiO_2 is one of the most complex and diverse material families, occurring naturally as a composite of multiple minerals and a synthesized material (glass former) [7, 8]. The mechanical, chemical, optical, and luminous properties of silicate glasses are outstanding. Silicates are

Address correspondence to E-mail: khattak.rajni@gmail.com

https://doi.org/10.1007/s10854-022-08194-w

essential components in industrial and domestic glassware [9]. It is employed in structural materials, microelectronics (as an electrical insulator), thermal and dielectric sectors, and components. Nanoparticle-doped silicate glasses can be used for various biomedical applications [10]. High density, optical absorption, and tunable refractive index are the outstanding features of bismuth-based glasses [11]. Bismuth has a number of important applications in glass and glass ceramics, thermal and mechanical detectors, reflecting windows, and optical and optoelectronic devices [12, 13]. Bismuth oxide can be used to synthesize glass materials, but glass formation is not easy. However, other compounds, such as PbO and SiO_2, can be used to grow glass materials by a simple synthesis pathway; these materials show structural units that are similar to BiO_3 and BiO_6. In BiO_3, the pyramidal structural unit is represented as a glass former in which the bismuth ion is attached to three oxygen atoms and the outermost lone pair of electrons $6s^2$ is present at the top. BiO_6 octahedral units act as modifiers and induce structural defects in the amorphous form [14–16]. It has been predicted that in glasses, bismuth oxide has dual role as a glass network and a modifier and this could be because of high polarizability and smaller ionic size of Bi^{3+}. Bismuth can also exist in different ionic states, such as Bi^{+}, Bi^{4+}, and Bi^{5+}, depending on its concentration and chemical composition [11, 17, 18]. When Bi_2O_3 is added to a silicate glass host, it transforms into a rigid, stretchy, non-corrosive, and thermally stable material. Because of their significant thermally stimulated luminescence, Bi_2O_3 dopant silicate glasses are commonly used as dosimeters for radiation therapy and protection. The addition of Bi_2O_3 to silicate glasses is suggested to enhance strength and provide gamma radiation protection [19]. PbO is another heavy metal oxide with a high atomic number, high refractive index, and low melting point [20]. Lead Oxide can be used as a filler/loading material in the matrix of various materials because it has an octahedral structure in its PbO_6 form, which can be used to improve material qualities; however, it has a covalent bond structure in its PbO_4 form, which can be used to grow glass materials [21–23]. Further, a high atomic weight of PbO and Bi_2O_3 in glass material expands the FTIR spectrum range and reveals different structural units [24]. Lithium ions, in addition to bismuth, have important applications due to their small size and ionic radii ($\approx$0.76 Å), electropositive nature, lightweight, ability to be used at high voltage, and high energy density [25, 26]. Lithium containing glasses can be utilized in solid-state lithium batteries and solid electrolytes because they have the highest ionic conductivity [27, 28]. Recently, Menazea et al. have reported the ac conductivity of lithium containing nanocomposite and found the suitability of material to be used in rechargeable battery applications [29]. Glass networks made of Bi_2O_3 and SiO_2 have been employed recently and the properties of these composites have been improved by adding lithium ions into a mixed matrix of Bi_2O_3 and SiO_2 [24, 30, 31]. All of the oxides mentioned above are commonly used to make high-resistance silicate-based compound glasses. Silicate-based glasses have a narrow cut-off wavelength and a large transmitting window, making them ideal for a variety of applications. Also, bismuth silicate glasses have essential applications, such as low-loss optical fibers, optical amplifiers, oscillators and IR transmitting materials [32, 33]. In the recent literature, there are several studies done on the glass systems Bi_2O_3-SiO_2 [34], $ZnO{\cdot}Bi_2O_3{\cdot}SiO_2$ [11], $PbO{\cdot}SiO_2$ [35], Bi_2O_3-$TiO_2{\cdot}SiO_2$ [36], $Li_2O{\cdot}Bi_2O_3{\cdot}SiO_2$ [37], $BaO{\cdot}Bi_2O_3{\cdot}SiO_2$ [38], $Li_2O{\cdot}PbO{\cdot}SiO_2$ [24], $Fe_2O_3{\cdot}Bi_2O_3{\cdot}SiO_2$ [39], SiO_2-$B_2O_3{\cdot}ZnO{\cdot}Bi_2O_3$ [19], $Li_2O{\cdot}ZnO{\cdot}Bi_2O_3{\cdot}SiO_2$ [40], and $Li_2O{\cdot}CdO{\cdot}Bi_2O_3{\cdot}SiO_2$ [41]. However, work on the physical, structural, and optical aspects of lithium lead bismuth silicate glass system has been not reported. Therefore, in the present research work, we synthesized $30Li_2O{\cdot}20PbO{\cdot}xBi_2O_3{\cdot}(50-x)SiO_2$ (where, x = 0 to 50 mol%) glasses and investigated the influence of bismuth oxide on the structural features of the samples by employing X-ray diffraction (XRD) and Fourier Transform Infrared (FTIR) Spectroscopy. In order to examine the role of different structural units spectra have been deconvoluted using origin software. A correlation between the physical and structural properties has been made. Further, for more insight optical properties viz., cut-off wavelength (λ_C), energy bandgap (E_g), Urbach energy (ΔE), theoretical optical basicity (Λ_{th}), oxide ions polarizability ($\alpha_0{}^{2-}$), refractive index (n), reflection loss (R_L), molar refractivity (R_m), and metallization criterion (M), using the UV–VIS–NIR spectroscopy have also been analyzed.

2 Experimental details

2.1 Synthesis of glasses

The chemicals required Li_2CO_3, $PbCO_3$, Bi_2O_3, and SiO_2 in the synthesis of desired samples were purchased from high media chemicals with 99.5% purity and analytical-grade mark. The glass samples were made using the melt-quenching technique with the composition $30Li_2O{\cdot}20PbO{\cdot}xBi_2O_3{\cdot}(50{-}x)SiO_2$ (where x = 0, 10, 20, 30, 40, and 50 mol%). The prepared mixture of chemicals was placed in a porcelain crucible and then heated in an electric muffle furnace at a temperature of 1150 °C. As obtained melt was occasionally stirred in between during the entire procedure of 30 min and we obtained homogeneous mixture. Finally, the resultant mixtures were splashed onto a stainless steel plate and pressed immediately with another stainless steel plate. The obtained samples were annealed below the glass transition temperature (T_g) for 3 h to remove thermal stress occurred during quenching. The prepared samples were labeled as S0, S1, S2, S3, S4, and S5.

2.2 Characterization techniques

The X-ray diffractograms of powdered samples were recorded at room temperature using a Rigaku Miniflex-II X-ray diffractometer. The glass transition temperature was recorded using a Differential Scanning Calorimeter (Model Mettler Toledo Q20) maintained at a temperature of 10 °C/min. For exploring the molecular bonding properties, Fourier transformation infrared spectroscopy was employed through PerkinElmer (BX-II) spectrometer at room temperature. For the FTIR measurements, acceptable glass powder samples were mixed with KBr in the proportion of 1:20. After preparing the thin pellets, the infrared spectra were recorded quickly to avoid moisture. The optical absorption spectra of the polished glass samples were recorded in the wavelength range of 190–3300 nm using a Shimadzu spectrometer (UV-3600 Plus).

3 Results and discussion

3.1 Structural and molecular bonding measurements

Figure 1a represents the XRD spectra of present glass samples (S0–S5). The XRD patterns of prepared samples were recorded between the angles 10 to 80°. Because of the highly short-range disordering of atoms in glasses, the XRD pattern of all the samples has a large hump around ~ 27° which confirms that the glass samples are amorphous in nature. Also, the variation is observed in the broad hump when loading takes place which confirms the fact of interaction between bismuth and silicate particles.

As shown in Fig. 1b, molecular bonding measurements were performed using FTIR in the

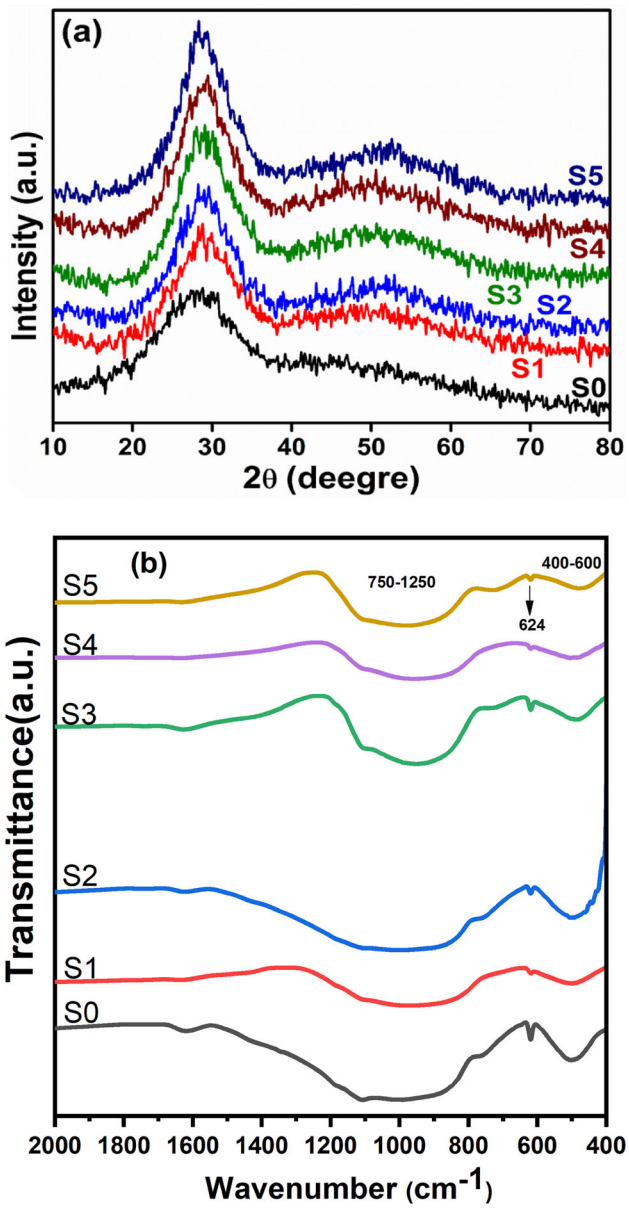

Fig. 1 **a** XRD patterns of different $30Li_2O{\cdot}20PbO{\cdot}xBi_2O_3{\cdot}(50-x){\cdot}SiO_2$ glass compositions. **b** FTIR spectra of different $30Li_2O{\cdot}20PbO{\cdot}xBi_2O_3$ $(50-x){\cdot}SiO_2$ glasses at room temperature

wavenumber range 400–2000 cm^{-1} at room temperature. This region of mid-infrared spectrum is the fingerprint region, where IR vibrations are most active. The FTIR spectra of present samples contain a number of fundamental bonds that confirm the desired samples growth. Due to the abundance of the heavy metal bismuth oxide (Bi_2O_3) and modifier cations (Li_2O, PbO), the position of absorption bands in the spectra of these glasses is similar to the usual ranges of lithium zinc bismuth silicate and borate glasses [40, 41]. Two absorption bands are identified in the wavelength range 750–1250 cm^{-1} centered at 981 cm^{-1} and 400–600 cm^{-1} centered at 498 cm^{-1}, respectively. From Fig. 1b, it is also observed that in the presence of a modifier, when the SiO_2 is replaced by an unusual glass former (Bi_2O_3) the intensity as well as the position of these bands changes. FTIR spectra in band range from 400 to 600 cm^{-1} infer that the band presents around wavenumber ~ 425 cm^{-1} as a result of symmetric oxygen bending-rock mode (*R*) BO's bonding and around ~ 450 cm^{-1} ascribed to the vibration of Pb–O in the PbO_4 structural unit [42, 43]. Furthermore, the Li–O–Li and Bi–O bending and stretching vibrations of bonds can be linked to the bands located between 400 and 600 cm^{-1} [44, 45]. Stalin et al. have assigned the band in this region to Li^+ and Bi–O–Bi linkage in BiO_6 octahedral unit [46]. Similarly, Kaur et al. have also linked the bands in region < 650 cm^{-1} to vibrations of the BiO_6 and in region 420–460 cm^{-1} to lithium cation vibration [47]. A sharp peak at 624 cm^{-1} is also observed behind this range, which shifts toward lower wavenumber when Bi_2O_3 percentage in glass composition increases and owing to Bi–O stretching vibrations in the BiO_6 octahedral unit [48]. A combined broad valley peak is observed in the wavenumber range 750–1250 cm^{-1}. To identify all present peaks in this region, this wavenumber range was deconvoluted into five components using Lorentzian and Gaussian curve fitting for all the samples. It is observed that the area under all of the bands change when the doping concentration of component increases, as shown in Fig. 2a–f. The calculated parameters such as peak position (X_c), amplitudes (*A*), the full width at half maxima (*W*), and the corresponding IR band assignments are tabulated in Tables 1 and 2, respectively. Figure 2a shows the deconvoluted FTIR spectra of pure ($x = 0$) samples, which consists of four peaks, whereas deconvoluted spectra of composite ($10 \leq x \leq 50$) samples contain five peaks indicating the development of a new peak when loading concentration is introduced in the matrix of the pure sample. In the deconvoluted spectra, the band at around ~ 868 cm^{-1} is attributed with the vibration of PbO_6 structural units and Bi–O stretching vibrations of Bi–O bonds in BiO_3 units [37, 45, 49], while band ~ 944 cm^{-1} is associated with O–Si–O bonds in $[SiO_4]^{4-}$ units (Q^0) stretch asymmetrically without bridging oxygen ions per silicon [35, 50]. Similarly, bands at 1029 cm^{-1} and 1104 cm^{-1} can be assigned to asymmetrical stretching vibrations of O–Si–O bonds in SiO_4 tetrahedral units in a pure sample. Peaks situated at around ~ 969 cm^{-1} may be assigned to the combined vibrations of PbO_6 structural units and asymmetric stretching vibrations of $[SiO_4]^{3-}$ units (Q^1; with one bridging oxygen ions per silicon) [51, 52]. Moreover, another band at around ~ 1035 cm^{-1} is due to the asymmetric stretching vibrations of $[SiO_4]^{2-}$ units (Q^2; with two bridging oxygen ions per silicon). However, another band observed at around ~ 1055 cm^{-1} is ascribed to the asymmetric stretching vibrations of $[SiO_4]^{-}$ units (Q^3; with three bridging oxygen ions per silicon). Also, the band situated at ~ 1105 cm^{-1} can be assigned to the linkage vibrations of Bi(3)–O–Bi(6) associated with NBOs and can be connected to the asymmetric stretching vibrations of $[SiO_4]$ tetrahedral units (Q^4; with four bridging oxygen ions per silicon) [52–54].

3.2 Physical properties

3.2.1 *Density measurements*

The density of the prepared samples was determined using the Archimedes principle at room temperature. Xylene was employed as the buoyant fluid in this technique. The adequate molar volume (V_m) for all the samples was estimated using the formula given below [11]

$$V_m = M/D, \quad (1)$$

where *M* is the molar mass, and *D* is the density of glass samples (*D* for xylene is 0.861 g/cm^3). The expressive crystalline volume (V_C) of samples was computed using the expression [11]

$$V_C = \sum x_i V_i, \quad (2)$$

Here x_i is the molar fraction and V_i is the crystalline molar volume for each constituents. For Li_2O, PbO,

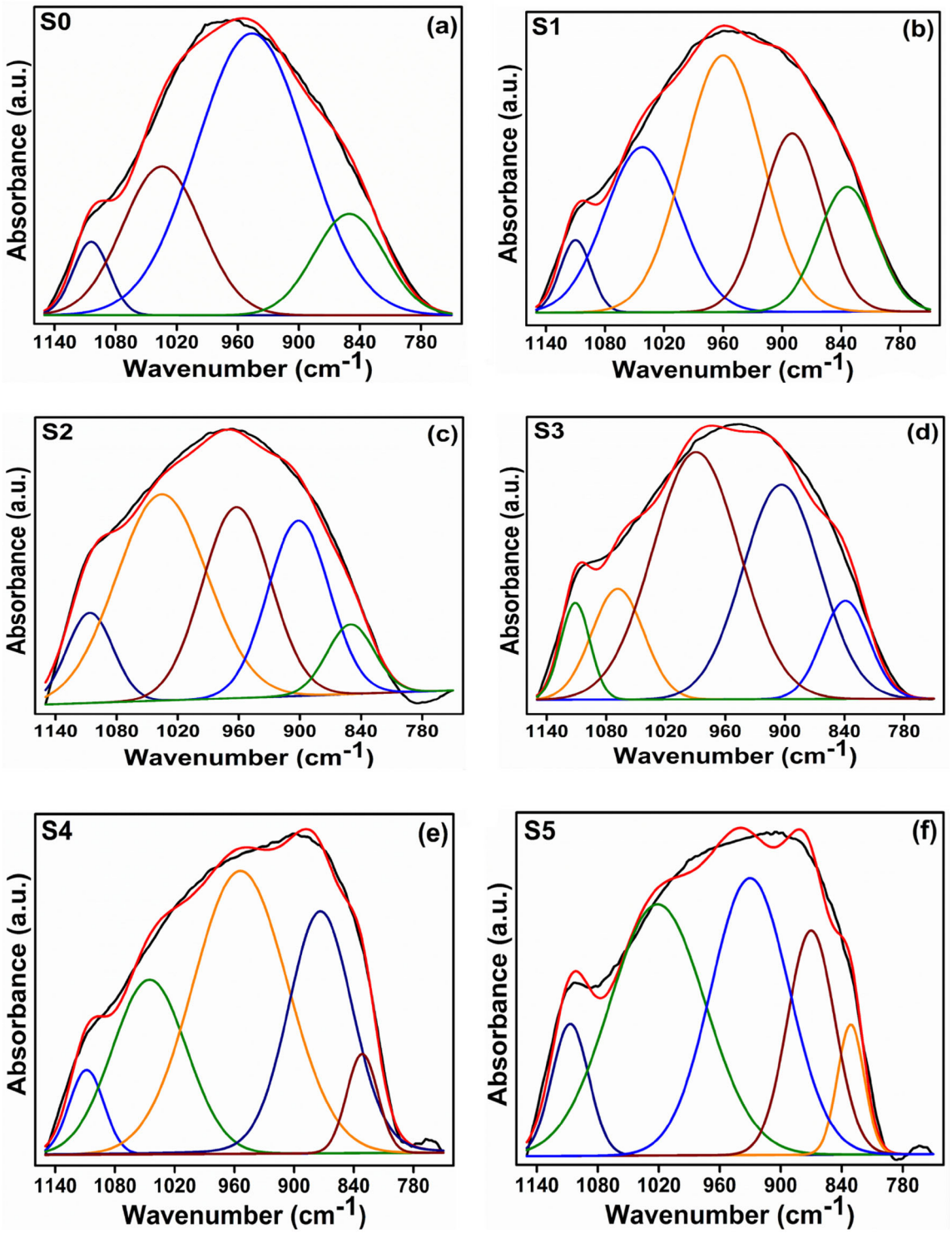

Fig. 2 **a**–**f** Deconvoluted FTIR spectra of $30Li_2O{\cdot}20PbO{\cdot}xBi_2O_3{\cdot}(50-x){\cdot}SiO_2$ glasses

Bi_2O_3, and SiO_2 crystalline molar volume is 14.84, 23.42, 52.36, and 22.68 cm^3, respectively [22].

Figure 3 illustrates that the density and the molar volume of the studied glasses show an increasing trend with the rise in concentration of Bi_2O_3. The values of density increase from 3.54 to 5.39 (g/cm^3) with the concentration of Bi_2O_3 (Table 3). Molar volume and crystalline volume show similar

Table 1 Peak position (X_c), Amplitude (A), and full width at half maxima (W) of deconvoluted peaks of FTIR spectra of different compositions of $30Li_2O{\cdot}20PbO{\cdot}xBi_2O_3{\cdot}(50-x){\cdot}SiO_2$ glass system

Peak	S0			S1			S2			S3			S4			S5		
No	X_C cm^{-1}	A a.u	W cm^{-1}	X_C cm^{-1}	A a.u	W cm^{-1}	X_C cm^{-1}	A a.u	W cm^{-1}	X_C cm^{-1}	A a.u	W cm^{-1}	X_C cm^{-1}	A a.u	W cm^{-1}	X_C cm^{-1}	A a.u	W cm^{-1}
1	1104	04	17	1107	03	04	1109	03	04	1108	02	04	1105	0.2	04	1109	0.4	04
2	1029	107	10	1040	24	10	1057	11	08	1054	07	07	1019	2.6	12	1042	1.7	10
3	944	217	13	959	37	10	969	25	11	992	09	07	934	1.6	09	964	1.9	09
4	868	58	09	889	20	08	892	07	07	934	10	07	870	1.5	07	889	02	08
5				834	12	07	849	02	04	854	11	09	831	0.3	04	840	0.4	04

Table 2 Data of FTIR spectra of $30Li_2O{\cdot}20PbO{\cdot}xBi_2O_3{\cdot}(50-x)SiO_2$ glasses (band position are in cm^{-1})

S0	S1	S2	S3	S4	S5	IR band assignments
868	834	–	–	831	–	PbO_6 bonds/Bi–O stretching vibration of Bi–O bonds in BiO_3 units [31, 40, 41]
–	–	849	854	–	840	Symmetric stretching vibration of Bi–O bonds in BiO_3 units [34]
–	889	892	–	870	889	The total symmetrical stretching vibrations of the $[BiO_3]$ and $[BiO_6]$ polyhedral [7, 41]
–	–	–	934	934	–	PbO_6 structural units [40]
944	–	–	–	–	–	Asymmetric stretching vibrations of $[SiO_4]^{4-}$ units (Q^0; without bridging oxygen ions per silicon) [29, 42]
–	959	969	992	–	964	PbO_6 structural units/asymmetric stretching vibrations of $[SiO_4]^{3-}$ units (Q^1; with one bridging oxygen ions per silicon) [43, 44]
1029	1040	–	–	1019	1042	Asymmetric stretching vibrations of $[SiO_4]^{2-}$ units (Q^2; with two bridging oxygen ions per silicon)
–	–	1057	1054	–	–	Asymmetric stretching vibrations of $[SiO_4]^{-}$ units (Q^3; with three bridging oxygen ions per silicon [44, 46]
1104	1107	1109	1108	1105	1109	Linkage vibrations of Bi(3)–O–Bi(6) [45]/asymmetric stretching vibrations of $[SiO_4]$ units (Q^4; with four bridging oxygen ions per silicon) [44, 46]

variations. The large molecular mass of bismuth (465.98 a.m.u) in comparison to silicate (60.08 a.m.u) entailed this increase in density and molar volume. Similar trends have been observed by Meena for bismuth containing glasses [9]. Also, there is no much variation in the density values after $x = 30$ shows some sort of structural changes occurring at this compositions. Further, for all glass compositions, V_m values exceed V_C values, indicating the existence of excess structural volume, i.e., the potential of glass formation rather than crystallization.

3.2.2 *Differential scanning calorimetry (DSC)*

The DSC thermographs of prepared glass samples are shown in Fig. 4. From these curves glass transition temperature for each composition was determined and values are listed in Table 3. The intensity of the chemical bond and the density of crosslinks in the glass matrix are hypothesized to affect the glass transition temperature [55]. The glass transition temperature increases with the bismuth concentration at the expense of silicate, as shown in Table 3. From density measurements, it can be predicted that as Bi_2O_3 content rise structure becomes more denser causing an increase in T_g. A slight decrease in the value of glass transition temperature for the S4 sample is due to the effect of Bi_2O_3 as a modifier usually weakening the glass structure, also confirmed by the FTIR spectra.

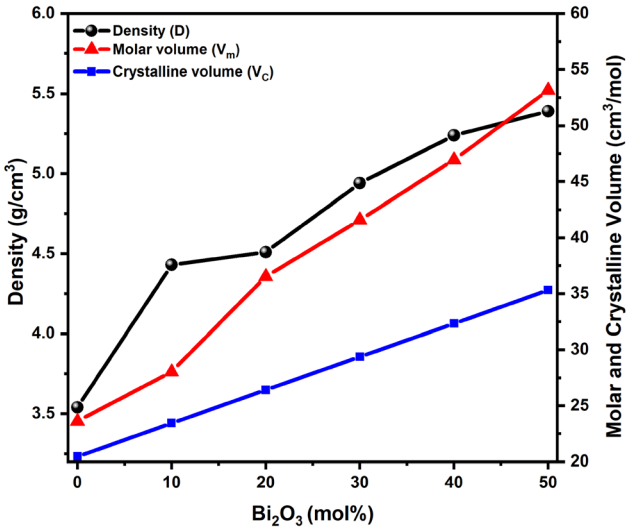

Fig. 3 Compositional dependency of density, molar volume, and crystalline volume for all the samples of $30Li_2O{\cdot}20PbO{\cdot}xBi_2O_3{\cdot}(50-x){\cdot}SiO_2$ glasses

Table 3 Physical and optical parameters of $30Li_2O{\cdot}20PbO{\cdot}xBi_2O_3{\cdot}(50-x)SiO_2$ glasses

Parameter	S0	S1	S2	S3	S4	S5
D (g/cm^3)	3.54	4.43	4.51	4.94	5.24	5.39
V_m (cm^3/mol)	23.63	28.04	36.55	41.58	46.95	53.17
V_C (cm^3/mol)	20.48	23.44	26.41	29.38	32.35	35.32
T_g (°C)	268	380	392	420	415	427
λ_C (nm)	358	410	418	446	482	539
E_g (eV) $n = 2$	3.11	2.68	2.48	2.30	2.12	1.92
ΔE (eV)	0.56	0.55	0.64	0.61	0.52	0.32
Λ_{th} $*(10^{-24}$ cm$^3)$	0.75	0.82	0.89	0.95	1.02	1.09
$\alpha_0{}^{2-}(E_g)$	1.77	1.94	2.11	2.31	2.56	2.87
n	2.38	2.51	2.56	2.66	2.71	2.77
R_L	0.17	0.18	0.19	0.20	0.21	0.22
R_m (cm^3/mol)	14.30	17.77	23.67	27.47	31.65	36.68
α_m	5.67	7.04	9.38	10.89	12.55	14.54
M	0.395	0.366	0.352	0.339	0.326	0.310

3.3 UV–VIS–NIR spectroscopy

3.3.1 *Optical absorption spectra*

In the present study, the optical bandgap and absorption coefficient, $\alpha(v)$ of glass samples were measured by studying the optical absorption spectra. The Beer–Lambert law is used to compute the absorption coefficient $\alpha(v)$,

$$\alpha(v) = \frac{A}{t}, \tag{3}$$

where A is the absorbance and t is the thickness of glass sample. A relationship between absorption coefficient $\alpha(v)$ and the role of photon energy (hv) gives the direct and indirect optical transitions as well as optical bandgap energy and is known as Tauc's relation [56].

$$\alpha(v) = \frac{B(hv - \mathrm{Eg})^n}{hv}, \tag{4}$$

where B is a constant and known as the band tailing parameter. The energy of photon is hv that is incident on glass materials and n is depending on the type of glass transition. The value of n = 2, 1/2, 3, and 1/3 depends upon the electronic transition of the absorption factor. For n = 2 and 3, transitions are considered as indirectly allowed and indirect forbidden, whereas for n = 1/2 and 1/3 transitions are directly allowed and direct forbidden, respectively [57]. Indirect optically allowed transition is possible in solid amorphous glass material. There are three regions found in the absorption coefficient. The first region is the high absorption region which is known as the "Tauc region" and depicted in Fig. 5. The energy gap of optical band was estimated from the linear section of the curve toward the energy axis at $(\alpha hv)^{1/2} = 0$ and obtained values are listed in Table 3. It is clear from Fig. 6, that with an increase in the concentration of Bi_2O_3 in the glass system, both the optical absorption spectra and the cut-off wavelength are observed to be red shifted. Similarly, the bandgap energy is seen to decrease from S0 (3.11 eV) to S5 (1.92 eV). This trend shows that when the concentration of bismuth ion rises (0 to 50 mol%), the non-bridging oxygen ion (NBO) rises, lowering the bandgap energy. Large difference in V_m and V_C values with increase in bismuth concentration also supports this assumption. The spectral investigations also revealed that NBOs are associated with asymmetrical stretching vibration in the SiO_4 tetrahedral unit. Because when a metal–oxygen bond breaks, bond energy is released. The highest energy state of the valence band model consists of O(2p) orbitals, whereas the lowest energy level is made up of the conduction band, which is made up of M(nS) orbitals. The non-bridging oxygen atoms have higher energy than bonding orbital. As a result, the increase in non-bridging oxygen (NBOs) concentration results in an

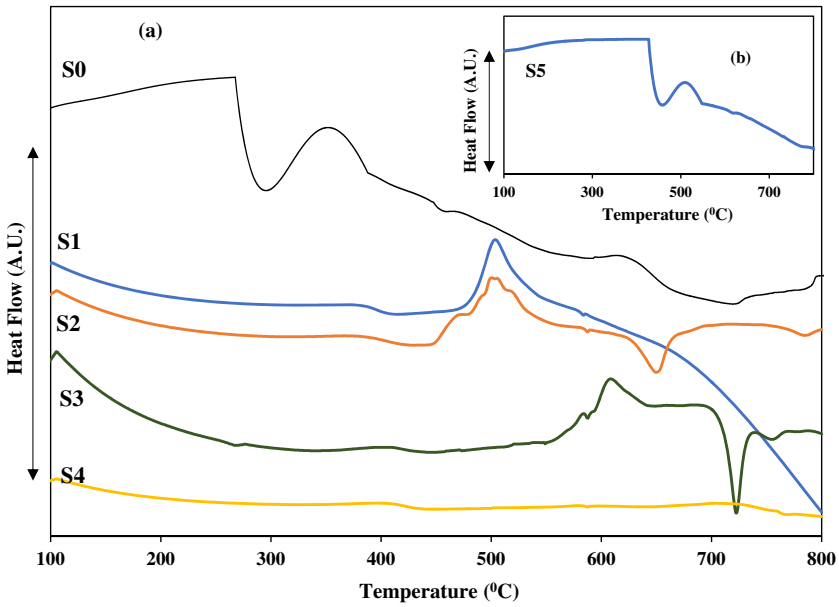

Fig. 4 DSC thermographs for different compositions of $30Li_2O{\cdot}20PbO{\cdot}xBi_2O_3{\cdot}(50-x){\cdot}SiO_2$ glasses

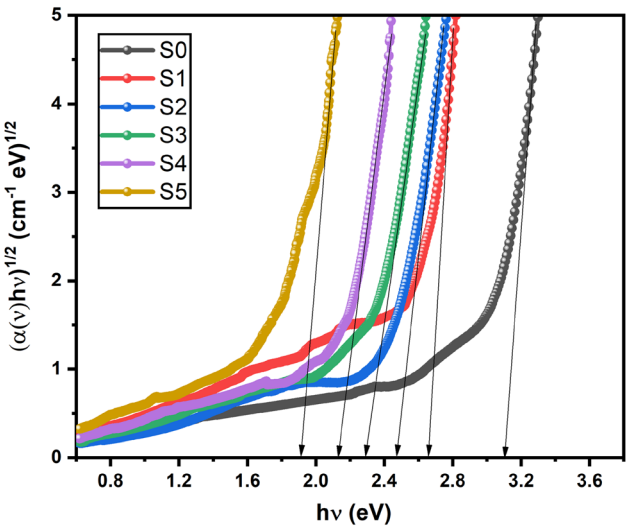

Fig. 5 Tauc's plot for all the compositions of $30Li_2O{\cdot}20PbO{\cdot}xBi_2O_3{\cdot}(50-x){\cdot}SiO_2$ glasses for $n = 2$

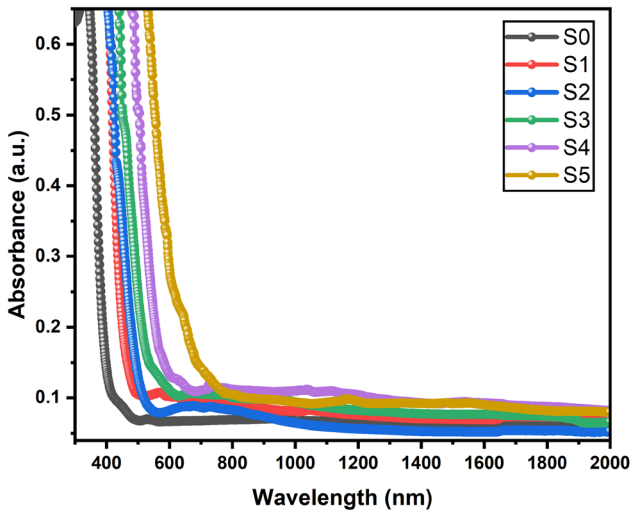

Fig. 6 Optical absorbance spectra as a function of wavelength for all compositions of $30Li_2O{\cdot}20PbO{\cdot}xBi_2O_3{\cdot}(50-x){\cdot}SiO_2$ glasses

increased VBM, lowering the optical bandgap energy [58]. Initially, polarization due to Bi^{3+} ions in the glass structure is modest at low content of Bi_2O_3 resulting in a small shift in the bandgap energy E_g. However, after adding Bi_2O_3, substantial polarization occurs owing to Bi^{3+} ions, leading to a large decrease in the bandgap energy E_g (Table 3). Thus, Bi_2O_3 enters the interstitial sites as a modifier upto 30 mol% that produces maximum NBOs. Bismuth ionic bonds are developed with NBOs at the place of covalent bonds. When the bismuth concentration is increased at 40 to 50 mol%, it enters in the network as a former. These results are also supported by the structural variation depending upon the composition in the present glasses.

The second region, known as the "Urbach region," appears as a result of structural disorientation of the materials. It depends on various factors, like thermal vibration in the lattice, temperature, statics, and induced disorder, and photon energy. The slope of the linear region curve drawn between ln(α) and $h\nu$, as illustrated in Fig. 7, was used to calculate the Urbach energy. The relationship can be expressed as,

$$\ln \alpha(v) = \frac{hv}{\Delta E} + \text{ constant.} \quad (5)$$

The obtained values of ΔE are presented in Table 3 and it was concluded that the value of ΔE decreases as the concentration of Bi_2O_3 content increases and the minimum value of Urbach energy is observed for S5. It may be due to the decrease in broadening that is correlated with the static disorder [59, 60]. The value of ΔE is consistent with the width of the band tail of the electron state. Due to phonon-assisted indirect electronic transition between localized states, the small value of ΔE generates the exponential tail [61]. Similarly, the significant value of ΔE reveals that defects are maximum and reduce the long-range order. In addition, as compared to other compositions, low values of Urbach energy at a high value of Bi_2O_3 suggest the possibility of long-range order locally developing the defect concentration [62].

The third region in UV spectra arises due to weak absorption. The values of refractive index increases and becomes maximum (Fig. 8) at a concentration of 50 mol% due to the maximum concentration of both modifier and former oxides of lead and bismuth. Also, a decrease in bandgap energy which causes an increase in refractive index is due to electronic band structure, as illustrated in Eq. (6)

$$\left(\frac{n^2-1}{n^2+2}\right) = 1 - \sqrt{\frac{E_g}{20}}. \quad (6)$$

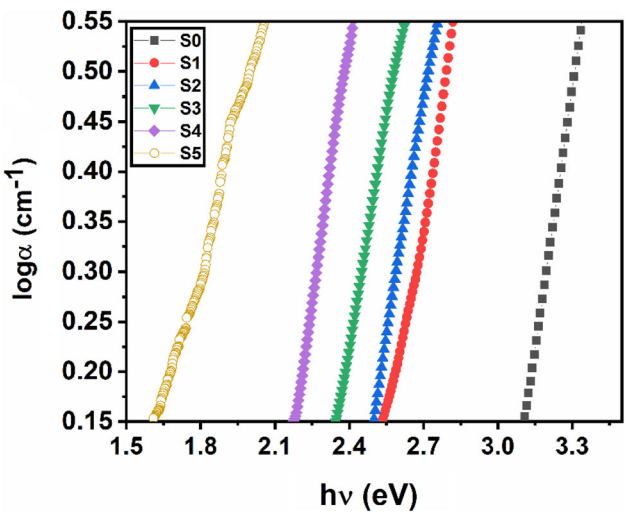

Fig. 7 Urbach's Plot for all the compositions of $30Li_2O{\cdot}20PbO{\cdot}xBi_2O_3{\cdot}(50-x){\cdot}SiO_2$ glasses

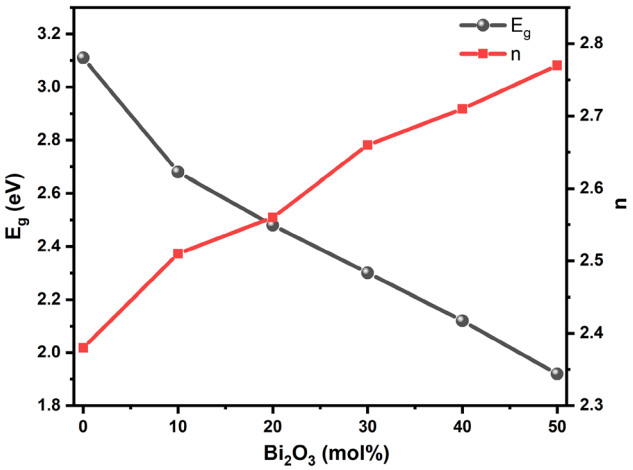

Fig. 8 The variation of bandgap energy and refractive index with different concentrations of Bi_2O_3

3.3.2 *Optical parameters*

The value of theoretical optical basicity (Λ_{th}) for the prepared glasses has been calculated by acid–base properties that represent in terms of electron density carries by oxygen using the expression (7) [63, 64].

$$\Lambda_{th} = \Lambda_{Li_2O}.X_{Li_2O} + \Lambda_{PbO}.X_{PbO} + \Lambda_{Bi_2O_3}.X_{Bi_2O_3} + \Lambda_{SiO_2}.X_{SiO_2}, \quad (7)$$

where $X_{Li_2O}, X_{PbO}, X_{Bi_2O_3}$, and X_{SiO_2} are equivalent fraction of different oxides and $\Lambda_{Li_2O}, \Lambda_{PbO}, \Lambda_{Bi_2O_3}$, and Λ_{SiO_2} are their optical basicities. The optical basicity values Λ_{Li_2O} = 0.87, Λ_{PbO} = 1.18, and $\Lambda_{Bi_2O_3}$ = 1.19, Λ_{SiO_2} = 0.50 are taken from the literature [65].

Simultaneously, it gives us a relationship between oxide ion polarizability (α_0^{2-}) and the optical basicity of the oxide medium,

$$\Lambda_{th} = 1.67\left(1 - \frac{1}{\alpha_0^{2-}}\right). \quad (8)$$

The value of theoretical optical basicity increases with the concentration of Bi_2O_3 content, as seen in Table 3. The polarizability of the Bi^{3+} cation is high, and it has a lone pair in the outermost shell. As a result, when the concentration of Bi_2O_3 increases, the NBOs and theoretical optical basicity increase. From Table 3 it can be seen that oxide ion polarizability also increases. The electron donor ability of the oxide ions is thought to be much more vital in these samples. The molar refractivity (R_m) is related to the polarizability of constituent ions of the glass and can be

computed from the E_g values, using the relation given as [66],

$$R_m = V_m\left[1-\sqrt{\frac{E_g}{20}}\right] = \left(\frac{n^2-1}{n^2+2}\right)\left(\frac{cm^3}{mol}\right). \quad (9)$$

The value of R_m increases with the increasing concentration of bismuth from 0 to 50 mol% rapidly and the reverse trend is observed in bandgap energy. The molar polarizability (α_m) is also related to molar refractivity as given by the relation [67],

$$\alpha_m = \left(\frac{3}{4\pi N_A}\right)R_m. \quad (10)$$

The reflection loss is also calculated by the given equation [62],

$$R_L = \left(\frac{n-1}{n+1}\right)^2. \quad (11)$$

The metallization criterion (M) of oxide based on its bandgap energy is given as [68],

$$M = 1-\frac{R_m}{V_m}. \quad (12)$$

Metallization criterion provides us the information on nature of the material. When the ratio of $R_m/V_m \geq 1$, the material is metallic in nature, and when the value of $R_m/V_m < 1$ material is of non-metallic nature. Table 3 shows that the reported values of M are less than 1, indicating that our samples are non-metallic in nature and may possess non-linear optical properties.

4 Conclusion

A study on the effect of substitution of SiO_2 by Bi_2O_3 on the physical and structural properties of $Li_2O{\cdot}PbO{\cdot}Bi_2O_3{\cdot}SiO_2$ glasses has been carried out. The diffused XRD patterns $\sim 27°$ confirm the amorphous nature of the as-prepared glass samples. The density, molar volume, and crystalline volume were increased with concentration of bismuth oxide. FTIR structural analysis reveals that Bi_2O_3 acts as network former and modifier and can exist in the structural units as BiO_3 and BiO_6. The indirect-allowed optical transition is possible in glass sample. For the present studied glass composition cut-off wavelength increases from 358 to 539 nm and bandgap energy decreases from 3.11 to 1.92 eV due to increase in bismuth concentration that increase the number of non-bridging oxygen ions which result in decrease of bandgap energy. The Urbach formula is used to determine Urbach energy. Smaller value ΔE at high Bi_2O_3 content shows the possibility of long-range order arising locally as the defect concentration grows. The values of metallization criterion for all the samples are less than 1 (0.395–0.310), which indicate that studied glasses can be explored for non-linear optical applications.

Author contributions

SC contributed to conceptualization, methodology, data curation, and writing of the original draft. RB contributed to supervision, methodology, and writing, reviewing, & editing of the manuscript. SR contributed to data curation. SG performed supervision and writing, reviewing, & editing of the manuscript.

Funding

The authors have not disclosed any funding.

Data availability

All the data analyzed in this work are included in this article. If more supporting information is required it can be available on request from the corresponding author (Dr. Rajni Bala).

Declarations

Conflict of interest The authors declare that they have no known competing financial interests or personal relationships that could have appeared to influence the work reported in this paper.

Ethical standards The contents of this research paper "Investigation of Structural and Optical Properties of Lithium Lead Bismuth Silicate Glasses" are new and we have synthesized these samples for the first time using melt-quenching technique. It is certified that the work is completely original and has not been published/submitted for publication elsewhere. We will follow all the norms of the publication, like copyrights.

References

1. O. Sanz, E. Haro-Poinatowski, J. Gonzalo, J.M. Fernandez Navarro, Influence of the melting conditions of heavy metal oxide glasses containing bismuth oxide on their optical absorption. J. Non-Cryst. Solids **352**, 761–768 (2006). https://doi.org/10.1016/j.jnoncrysol.2006.02.002
2. W.H. Dumbaugh, J.C. Lapp, Heavy metal oxide glasses. J. Am. Ceram. Soc. **75**(9), 2315–2326 (1992). https://doi.org/10.1111/j.1151-2916.1992.tb05581.x
3. R. Bala, A. Agarwal, S. Sanghi, N. Singh, Effect of Bi_2O_3 on nonlinear optical properties of $ZnO{\cdot}Bi_2O_3{\cdot}SiO_2$ glasses. Opt. Mater. **36**(2), 352–356 (2013). https://doi.org/10.1016/j.optmat.2013.09.021
4. M.G. Dong, O. Agar, H.O. Tekin, O. Kilicoglu, K.M. Kaky, M.I. Sayyed, A comparative study on gamma photon shielding features of various germanate glass systems. Compos. B. Eng. **165**, 636–647 (2019). https://doi.org/10.1016/j.compositesb.2019.02.022
5. M.I. Sayyed, G. Lakshminarayana, M.G. Dong, M. Çelikbilek-Ersundu, A.E. Ersundu, I.V. Kityk, Investigation on gamma and neutron radiation shielding parameters for $BaO/SrO-Bi_2O_3-B_2O_3$ glasses. Radiat. Phys. Chem. **145**, 26–33 (2018). https://doi.org/10.1016/j.radphyschem.2017.12.010
6. M. Kurudirek, Heavy metal borate glasses: potential use for radiation shielding. J. Alloys Compd. **727**, 1227–1236 (2017). https://doi.org/10.1016/j.jallcom.2017.08.237
7. A.F.A. El-Rehim, E.A.A. Wahab, M.M.A. Halaka, K.S. Shaaban, Optical properties of SiO_2-TiO_2-La_2O_3-Na_2O-Y_2O_3 glasses and a novel process of preparing the parent glass-ceramics. SILICON **14**, 373–384 (2022). https://doi.org/10.1007/s12633-021-01002-w
8. X. Lu, L. Zhang, H. Talebinezhad, Y. Tong, Z.Y. Cheng, Effects of CuO additive on the dielectric property and energy-storage performance of $BaTiO_3$-SiO_2 ceramic-glass composite. Ceram. Int. **44**(14), 16977–16983 (2018). https://doi.org/10.1016/j.ceramint.2018.06.139
9. S.L. Meena, Thermal and physical properties of Pm^{3+} ions doped lead lithium bismuth silicate glasses. J. Pure Appl. Ind. Phys. **9**(11), 72–81 (2019)
10. A.A. Menazea, A.M. Abdelghany, Precipitation of silver nanoparticle within silicate glassy matrix via Nd:YAG laser for biomedical applications. Rad. Phys. Chem. **174**, 108958 (2020). https://doi.org/10.1016/j.radphyschem.2020.108958
11. R. Bala, A. Agarwal, S. Sanghi, S. Khasa, Influence of SiO_2 on the structural and dielectric properties of $ZnO{\cdot}Bi_2O_3{\cdot}SiO_2$ glasses. J. Integr. Sci. Technol. **3**(1), 6–13 (2015)
12. S. Sailaja, C.N. Raju, C.A. Reddy, B.D.P. Raju, Y.D. Jho, S. Reddy, Optical properties of Sm^{3+}-doped cadmium bismuth borate glasses. J. Mol. Struct. **1038**, 29–34 (2013). https://doi.org/10.1016/j.molstruc.2013.01.052
13. A. Dutta, A. Ghosh, Structural and optical properties of lithium barium bismuthate glasses. J. Non-Cryst. Solids **353**, 1333–1336 (2007). https://doi.org/10.1016/j.jnoncrysol.2006.09.052
14. S.M. Abo-Naf, R.L. Elwan, G.M. Elkomy, Crystallization of bismuth oxide nano-crystallites in a SiO_2-PbO-Bi_2O_3 glass matrix. J. Non-Cryst. Solids **358**(5), 964–968 (2012). https://doi.org/10.1016/j.jnoncrysol.2012.01.034
15. T. Maeder, Review of Bi_2O_3 based glasses for electronics and related applications. Int. Mater. Rev. **58**(1), 3–40 (2013). https://doi.org/10.1179/1743280412Y.0000000010
16. W. Vogel, *Glass Chemistry*, 2nd edn. (Springer, Berlin, 1994)
17. Y.B. Saddeek, G.Y. Mohamed, H.S. Hassan, A.M.A. Mostafa, G. Abdelfadeel, Effect of gamma irradiation on the FTIR of cement kiln dust– bismuth borate glasses. J. Non-Cryst. Solids **419**(1), 110–117 (2015). https://doi.org/10.1016/j.jnoncrysol.2015.03.021
18. L. Baia, R. Stefan, W. Kiefer, J. Popp, S. Simon, Structural investigations of copper doped B_2O_3-Bi_2O_3 glasses with high bismuth oxide content. J. Non-Cryst. Solids **303**, 379–386 (2002). https://doi.org/10.1016/S0022-3093(02)01042-6
19. Y.-S. Lai, S.-S. Lai, Y.-J. Lie, H.-J. Lin, T.-H. Chiang, Investigation of SiO_2-B_2O_3-ZnO-Bi_2O_3 glass frits on the interface reaction of silver front contacts. J. Alloys Compd. **858**, 157646 (2021). https://doi.org/10.1016/j.jallcom.2020.157646
20. S.M. Saheb, P.V. Rao, R. Vijay, P.R. Babu, Ch. Chandrakala, P.S. Prasad, G.N. Raju, Spectroscopic and electrical investigations of copper ions in PbO–GeO_2 glasses. Results Phys. **11**, 780–786 (2018). https://doi.org/10.1016/j.rinp.2018.10.012
21. A. Pan, A. Ghosh, Dynamics of lithium ions in bismuthate glasses. J. Chem. Phys. **112**, 1503 (2000). https://doi.org/10.1063/1.480717
22. A. Dutta, A. Ghosh, Ionic conductivity of Li_2O-BaO-Bi_2O_3 glasses. J. Non-Cryst. Solids **351**, 203–208 (2005). https://doi.org/10.1016/j.jnoncrysol.2004.11.010
23. A.V. Rao, C. Laxmikanth, B.A. Rao, N. Veeraiah, Dielectric relaxation and a.c. conduction phenomena of PbO–PbF_2–B_2O_3 glasses doped with FeO. J. Phys. Chem. Solids **67**, 2263–2274 (2006). https://doi.org/10.1016/j.jpcs.2006.04.012
24. N. Ahlawat, N. Ahlawat, A. Agarwal, P. Aghamkar, Monica, Infrared spectroscopic study for structural investigation of lithium lead silicate glasses. AIP Conf. Proc. **1393**, 313–314 (2011). https://doi.org/10.1063/1.3653735
25. K.J. Rao, B.G. Rao, S.R. Elliott, Glass formation in the system PbO-$PbCl_2$. J. Mater. Sci. **20**, 1678–1682 (1985). https://doi.org/10.1007/BF00555271

26. G. Srinivasa Rao, N. Veeraiah, Study on various physical properties of PbO–As_2O_3 glasses containing manganese ions. J. Alloys Compd. **327**(1–2), 52–65 (2001). https://doi.org/10.1016/S0925-8388(01)01559-6
27. J. Yao, Y. Li, R.C. Massé, E. Uchaker, G. Cao, Revitalized interest in vanadium pentoxide as cathode material for lithium-ion batteries and beyond. Energy Storage Mater. **11**, 205–259 (2018). https://doi.org/10.1016/j.ensm.2017.10.014
28. A. Kato, M. Yamamoto, A. Sakuda, A. Hayashi, Mechanical properties of Li_2S-P_2S_5 glasses with lithium halides and application in all-solid-state batteries. ACS Appl. Energy Mater. **1**, 1002–1007 (2018). https://doi.org/10.1021/acsaem.7b00140
29. A.A. Menazea, A.M. Ismail, I.S. Elashmawi, The role of $Li_4Ti_5O_{12}$ nanoparticles on enhancement the performance of PVDF/PVK blend for lithium-ion batteries. J. Mater. Res. Technol. **9**(3), 5689–5698 (2020). https://doi.org/10.1016/j.jmrt.2020.03.093
30. H. Masai, Y. Takahashi, T. Fujiwara, T. Suzuki, Y. Ohishi, Correlation between near infrared emission and bismuth radical species of Bi_2O_3-containing aluminoborate glass. J. Appl. Phys. **106**, 103523 (2009). https://doi.org/10.1063/1.3264631
31. A.R. Molla, A. Tarafder, B. Karmakar, Synthesis and properties of glasses in the K_2O–SiO_2–Bi_2O_3–TiO_2 system and bismuth titanate ($Bi_4Ti_3O_{12}$) nano glass–ceramics thereof. J. Mater. Sci. **46**, 2967–2976 (2011). https://doi.org/10.1007/S10853-010-5173-1
32. K.J. Rao, *Structural Chemisstry of Glasses* (Elsevier, North Holland, 2002). https://doi.org/10.1016/B978-0-08-043958-7.X5017-1
33. Y. Chu, J. Ren, J. Zhang, G. Peng, J. Yang, P. Wang, L. Yuan, Ce^{3+}/Yb^{3+}/Er^{3+} triply doped bismuth borosilicate glass: a potential fiber material for broadband near-infrared fiber amplifiers. Sci. Rep. **6**, 33865 (2016). https://doi.org/10.1038/srep33865
34. B. Bochentyn, A. Warych, N. Szreder, A. Mielewczyk-Gryn, J. Karczewski, M. Przesniak-Welenc, M. Gazda, B. Kusz, Characterization of structural, thermal and mechanical properties of bismuth silicate glasses. J. Non-Cryst. Solids **439**, 51–56 (2016). https://doi.org/10.1016/j.jnoncrysol.2016.02.026
35. I.B. Kacem, L. Gautron, D. Coillot, D.R. Neuville, Structure and properties of lead silicate glasses and melts. Chem. Geol. **461**, 104–114 (2017). https://doi.org/10.1016/j.chemgeo.2017.03.030
36. S.S. Slavov, Y.B. Dimitriev, Glass formation in the system Bi_2O_3-TiO_2-SiO_2. J. Chem. Technol. Metall. **51**, 536–546 (2016)
37. N. Ahlawat, S. Sanghi, A. Agarwal, R. Bala, Influence of SiO_2 on the structure and optical properties of lithium bismuth silicate glasses. J. Mol. Struct. **963**, 82–86 (2010). https://doi.org/10.1016/j.molstruc.2009.10.018
38. J. Ren, J. Qiu, D. Chen, C. Wang, X. Jiang, C. Zhu, Infrared luminescence properties of bismuth-doped barium silicate glasses. J. Mater. Res. **22**, 1954–1958 (2007). https://doi.org/10.1557/jmr.2007.0245
39. R. Parmar, R.S. Kundu, R. Punia, P. Aghamkar, N. Kishore, Iron modified structural and optical spectral properties of bismuth silicate glasses. Phys. Rev. B Condens. Matter **450**(1), 39–44 (2014). https://doi.org/10.1016/j.physb.2014.05.056
40. S. Rani, S. Sanghi, N. Ahlawat, A. Agarwal, Influence of Bi_2O_3 on thermal, structural and dielectric properties of lithium zinc bismuth borate glasses. J. Alloys Compd. **597**, 110–118 (2014). https://doi.org/10.1016/j.jallcom.2014.01.211
41. S. Rani, S. Sanghi, N. Ahlawat, A. Agarwal, Crystallization kinetics, optical and dielectric properties of $Li_2O{\cdot}CdO{\cdot}Bi_2O_3{\cdot}SiO_2$ glasses. J. Mol. Struct. **1098**, 1–11 (2015). https://doi.org/10.1016/j.molstruc.2015.05.017
42. N. Ahlawat, S. Sanghi, A. Agarwal, S. Rani, Effect of Li_2O on structure and optical properties of lithium bismosilicate glasses. J. Alloys Compd. **480**, 516–520 (2015). https://doi.org/10.1016/j.jallcom.2009.01.116
43. H.A. Othman, H.S. Elkholy, I.Z. Hager, FTIR of binary lead borate glass: Structural investigation. J. Mol. Struct. **1106**, 286–290 (2016). https://doi.org/10.1016/j.molstruc.2015.10.076
44. A.M. Abdelghany, H.A. ElBatal, R.M. Ramadan, The effect of Li_2O and LiF on structural properties of cobalt doped borate glasses. J. King Saud Univ. Sci. **29**(4), 510–516 (2017). https://doi.org/10.1016/j.jksus.2016.09.003
45. C.H. Rajyasree, P.M.V. Teja, K.V.R. Murthy, D.K. Rao, Optical and other spectroscopic studies of lead, zinc bismuth borate glasses doped with CuO. Phys. Rev. B Condens. Matter **406**, 4366–4372 (2011). https://doi.org/10.1016/j.physb.2011.08.082
46. S. Stalin, D.K. Gaikwad, M.S. Al-Buriahi, Ch. Srinivasu, S.A. Ahmed, H.O. Tekin, S. Rahman, Influence of Bi_2O_3/WO_3 substitution on the optical, mechanical, chemical durability and gamma ray shielding properties of lithium-borate glasses. Ceram. Int. **47**, 5286–5299 (2021). https://doi.org/10.1016/j.ceramint.2020.10.109
47. P. Kaur, K.J. Singh, S. Thakur, M. Kurudirek, M.M. Rafiei, Structural investigation and nuclear radiation shielding ability of bismuth lithium antimony borate glasses. J. Phys. Chem. Solids **150**, 109812 (2021). https://doi.org/10.1016/j.jpcs.2020.109812

48. M.A. Girsova, S.V. Firstov, T.V. Antropova, Structural and optical properties of the bismuth-containing quartz-like glasses. J. Phys.: Conf. Ser. **541**, 012022 (2014). https://doi.org/10.1088/1742-6596/541/1/012022
49. P. Pascuta, M. Bosca, S. Rada, M. Culea, I. Bratu, E. Culea, FTIR spectroscopic study of Gd_2O_3-Bi_2O_3-B_2O_3 glasses. J. Optoelectron. Adv. Mater. **10**, 2416–2419 (2008)
50. B. Suresh, M.S. Reddy, A.S.S. Reddy, Y. Gandhi, V.R. Kumar, N. Veeraiah, Spectroscopic features of Ni^{2+} ion in PbO–Bi_2O_3–SiO_2 glass system. Spectrochem. Acta Part A: Mol. Biomol. Spectrosc. **141**, 263–271 (2015). https://doi.org/10.1016/j.saa.2015.01.058
51. M. Bosca, L. Pop, G. Borodi, P. Pascuta, E. Culea, XRD and FTIR structural investigations of erbium-doped bismuth-lead-silver glasses and glass ceramics. J. Alloys Compd. **479**, 579–582 (2009). https://doi.org/10.1016/j.jallcom.2009.01.001
52. K.H. Sun, Fundamental condition of glass formation. J. Am. Ceram. Soc. **30**(9), 277–281 (1947). https://doi.org/10.1111/j.1151-2916.1947.tb19654.x
53. S.S. Rojas, J.E. Souza, M.R.B. Andreeta, A.C. Hernandes, Influence of ceria addition on thermal properties and local structure of bismuth germanate glasses. J. Non-Cryst. Solids **356**, 2942–2946 (2010). https://doi.org/10.1016/j.jnoncrysol.2010.05.101
54. A.S. Tenney, J. Wong, Vibrational spectra of vapor-deposited binary borosilicate glasses. J. Chem. Phys. **56**, 5516 (1972). https://doi.org/10.1063/1.1677069
55. M.A. Baki, F.A.A. Wahab, F. El. Diasty, One-photon band gap engineering of borate glass doped with ZnO for photonics applications. J. Appl. Phys. **111**, 073506 (2012). https://doi.org/10.1063/1.3698623
56. J. Tauc, Absorption edge and internal electric fields in amorphous semiconductors. Mater. Res. Bull. **5**, 721–729 (1970). https://doi.org/10.1016/0025-5408(70)90112-1
57. R. Jose, T. Suzuki, Y. Ohishi, Thermal and optical properties of TeO_2-BaO-SrO-Nb_2O_5 based glasses: new broadband Raman gain media. J. Non-Cryst. Solids **352**, 5564–5571 (2006). https://doi.org/10.1016/j.jnoncrysol.2006.09.013
58. L. Skuja, K. Kajihara, Y. Ikuta, M. Hirano, H. Hosono, Urbach absorption edge of silica: reduction of glassy disorder by fluorine doping. J. Non-Cryst. Solids **345**, 328–331 (2004). https://doi.org/10.1016/j.jnoncrysol.2004.08.038
59. B. Jarzabek, J. Weszka, J. Cisowski, Distribution of electronic states in amorphous Cd–As thin films on the basis of optical measurements. J. Non-Cryst. Solids **333**, 206–211 (2004). https://doi.org/10.1016/j.jnoncrysol.2003.09.045
60. S. Sanghi, S. Duhan, A. Agarwal, P. Aghamkar, Study of structure and optical properties of Fe_2O_3·CaO·Bi_2O_3 glasses. J. Alloys Compd. **488**, 454–458 (2009). https://doi.org/10.1016/j.jallcom.2009.09.009
61. N. Ahlawat, S. Sanghi, A. Agarwal, N. Ahlawat, Influence of SiO_2 on dispersive conductivity and absorption edge of calcium bismuthate glasses. Solid State Ion. **204**, 20–26 (2011). https://doi.org/10.1016/j.ssi.2011.08.018
62. F. Zaman, G. Rooh, N. Srisittipokakun, C. Wongdeeying, H.J. Kim, J. Kaewkhao, Physical, structural and luminescence investigation of Eu^{3+}-doped lithium-gadolinium bismuth-borate glasses for LEDs. Solid State Sci. **80**, 161–169 (2018). https://doi.org/10.1016/j.solidstatesciences.2018.04.010
63. J.A. Duffy, M.D. Ingram, Establishment of an optical scale for Lewis basicity in inorganic oxyacids, molten salts, and glasses. J. Am. Chem. Soc. **93**, 6448–6454 (1971). https://doi.org/10.1021/ja00753a019
64. J.A. Duffy, M.D. Ingram, An interpretation of glass chemistry in terms of the optical basicity concept. J. Non-Cryst. Solids. **21**, 373–410 (1976). https://doi.org/10.1016/0022-3093(76)90027-2
65. V. Dimitrov, T. Komatsu, Classification of simple oxides: a polarizability approach. J. Solid State Chem. **163**, 100–112 (2002). https://doi.org/10.1006/jssc.2001.9378
66. S. Bale, N.S. Rao, S. Rahman, Spectroscopic studies of Bi_2O_3-Li_2O-ZnO-B_2O_3 glasses. Solid State Sci. **10**, 326–331 (2008). https://doi.org/10.1016/j.solidstatesciences.2007.09.017
67. V. Dimitrov, T. Komatsu, Electronic polarizability, optical basicity and non-linear optical properties of oxide glasses. J. Non-Cryst. Solids **249**, 160–179 (1999). https://doi.org/10.1016/S0022-3093(99)00317-8
68. F. El-Diasty, F.A. AbdelWahab, M. Abdel-Baki, Optical band gap studies on lithium aluminum silicate glasses doped with Cr^{3+} ions. J. Appl. Phys. **100**, 093511 (2006). https://doi.org/10.1063/1.2362926